Electrical transport phenomena in nanostructured porous-silicon films

M. A. Vásquez
Facultad de Ciencias de la Electrónica, Benemérita Universidad Autónoma de Puebla, 72000, Puebla, México.
e-mail: mava.vasquez@gmail.com

G. Romero-Paredes and R. Peña-Sierra
Centro de Investigación y de Estudios Avanzados del Instituto Politécnico Nacional, Depto. de Ing. Eléctrica, SEES. Apartado Postal 14-740, Ciudad de México, 07000, México,
e-mail: rpsierra@cinvestav.mx

Received 11 June 2018; accepted 11 August 2018

The charge transport mechanisms in nanostructured porous silicon (PS) films were studied through current-voltage (I-V) measurements of planar Au/PS/Au structures in dark conditions at 300 K. The films were formed by electrochemical etching of $1-5$ Ω-cm p-type Si (100) wafers producing PS layers of 4.48×10^{9} Ω-cm. The charge transport is limited both by the space charge limited currents (SCLC) and the carrier trapping- detrapping kinetics in the inherent localized PS energy levels. I-V characteristics evolve according to the trapping-detrapping carrier kinetics in the films showing that applying external bias, the electrical current can be controlled. For the first time the trap filling limiting voltage (V_{TFL}) was identified in PS films that shift between 1 and 3 volts by the carrier trapping-detrapping kinetics from the PS intrinsic defect states. An energy band diagram for the films is schematically depicted including defect states. To give a reasonable explanation of the found behavior the existence of a thin silicon oxide film covering the network-like-silicon-nanocrystallites is required, in agreement with the widely accepted PS film structural models.

Keywords: Porous silicon films; metal-insulator-metal structures; electrical characteristics; space charge limited current (SCLC); V_{TFL}; electronic transport in interface structures.

PACS: 81.07.-b; 84.37.+q; 73.40.-c; 73.40.Rw.

1. Introduction

A variety of semiconductor structures have been proposed to be used as resistive random access memories (RRAM) for the next generation of non-volatile memories. Resistive switching structures must possess low power consumption produced by functional fabrication methods; in this line simple SiO_2 based structures should be advantageous [1,2]. Relatively complex materials systems offer apparent advantages in comparison with the mature metal/silicon-oxide technology, however the current transport mechanisms in Si-SiO_2 based structures must be studied to clarify non-well understood phenomena to promote its application in advanced resistive switching devices. For example switching phenomena have been explained in part by positive charges storage effects that have been demonstrated in metal/SiO_x/metal structures [3], but also by explanations involving non well-known mechanisms at the interphases or surfaces in nanoscopic structures. Nowadays three mechanisms are widely accepted to explain electrical switching phenomena; ionic, thermal and electronic. In this context, porous silicon (PS) films has been gaining relevance as a material for electronic resistive switching applications using its network-like-silicon- nanocrystallites arrangement covered by a non-stoichiometry silicon oxide (SiOx) thin film. Nanostructured PS films have been proposed to fabricate devices as light emitting diodes (LED's) [4], solar cells [5], supercapacitors [6,7], etc. however, until now the charge transport mechanism in the PS films associated to the resistive switching phenomena even requires more work to be clarified. Conduction mechanism as the Schottky effect, Poole- Frenkel, Tunneling, Space Charge Limit Current (SCLC) transport, and the injection power law regime have been suggested as the mechanisms controlling the current flow in PS films based structures [8], but the conduction regime linked to the electrical properties has not been fully discussed. For example, among the proposed electrical conduction mechanisms there exist certain degree of inaccuracy because diverse factors such as chemical reactivity, the local electric fields and Joule heating are usually claimed to explain experimental observations [9]. One of the factors that define the PS electrical conduction mechanisms is the huge concentration of trapping centers that can exceed $\sim 10^{19}$ cm^{-3} [10], but its effects have not been fully discussed.

In this work, the current-voltage (I-V) characteristics of planar Au/PS/Au structures were studied with the aim to identify the dominant carrier transport mechanisms in the PS films. On the basis of previous studies and the measured I-V characteristics, a qualitative model is proposed to explain the electrical behavior of the PS films of enough length to discard the influence of the Au/PS electrodes.

2. Experimental

The PS films to build the Au/PS/Au planar structures were prepared on $1-5$ Ω-cm p-type Si (100) wafers by anodic etching using a home-made all Teflon electrochemical cell,

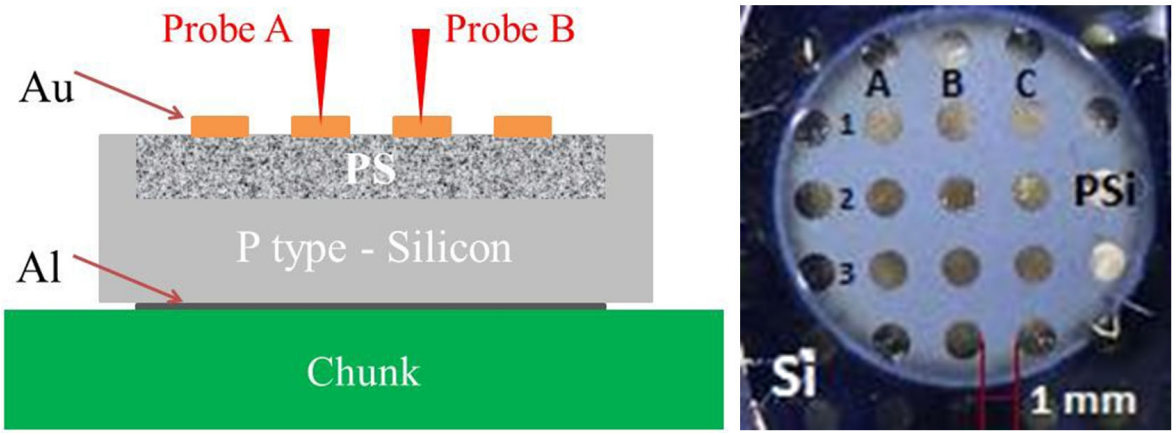

FIGURE 1. Sketch of the planar Au/PS/Au structure fabricated on PS films to study the electrical transport mechanisms in the PS films.

the complete description of the used process was described in a previous work [11]. The etching was carried out in a Hydrofluoric Acid (48%): Ethanol (1:1) solution, with a current density of 10 mA cm^{-2} by 15 sec. After the anodization process the samples were rinsed with ethanol and dried with N_2 gas flow. With these conditions PS films with a porosity of $\sim$ 95 % of 60 nanometer (nm) in thickness were produced as estimated by ellipsometric measurements [11]. The morphology of the PS samples surface were analyzed using a field-emission scanning electron microscope (FESEM) AURIGA 3916-FESEM with an operating voltage between 1 to 2 kV; surface chemical analysis on the samples was made by EDS in the same facility.

The average size of the silicon crystallites forming the PS films was experimentally estimated through photoluminescence (PL) measurements at room temperature using a system based on a double monochromator SPEX model 1404 with 0.8 m of focal length. The PL signal was excited with the line 488 nm of an Argon laser of 4W and detected with a type S1 photomultiplier tube.

The Au/PS/Au planar structures were produced by depositing circular shaped gold (Au) electrodes of 500 nm in thickness and 1 mm in diameter on the PS surface by vacuum evaporation at 10^{-5} Torr. The Au electrodes separated 1 mm arranged in a matrix array are depicted in the Fig. 1. Current-Voltage (I-V) characteristics produced by the PS films of the Au/PS/Au planar structures were taken in the forward bias regime in the low electrical field regime ($< 2\times10^2$ V/cm) applying two measurement modes to fix the initial charge state condition to study the electrical transport mechanisms of the PS layers. The data was taken at 300 K in dark conditions using a Keithley semiconductor characterization system model 4200-SCS. Because distance between the Au electrodes is the larger the recognized high resistance of the PS film leads to discard the role of both Metal-PS electrodes, and to consider firstly that the PS film controls the carrier transport. The two measurements modes were applied in sequence; in the first mode empty traps initial condition was fixed by short circuiting the pair of used electrodes, for example the electrodes

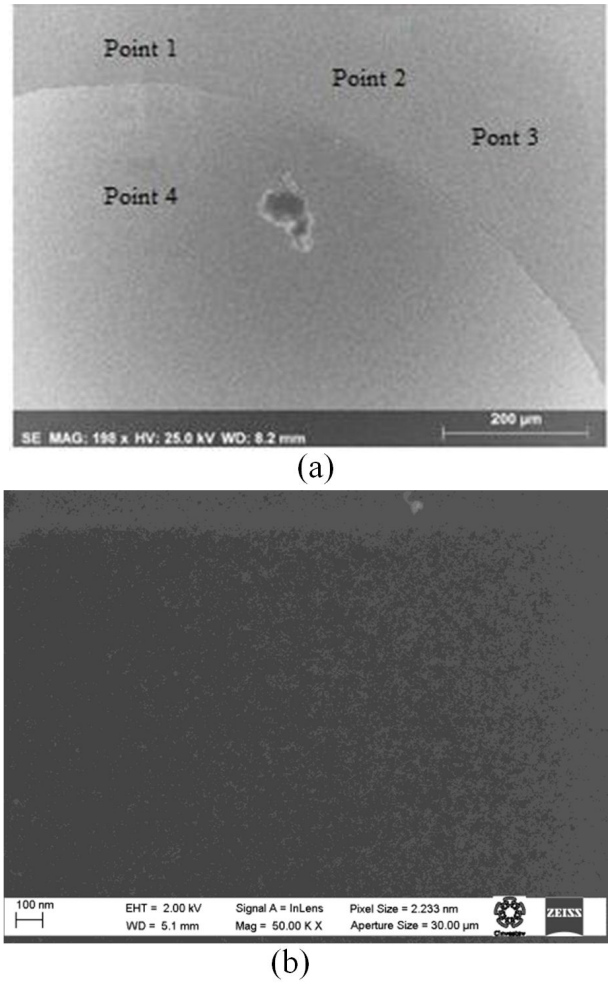

FIGURE 2. Scanning electron microscopy (SEM) microphotographs images taken over the PS vicinal area of a circular shaped Au electrode shown in the Fig. 1. (a) Four points are marked were EDS analysis where done to known the surface chemical of the samples. (b) Detail of the PS surface for the Point 2 with a 50.00 X magnification.

A1 and B1 seen in Fig. 1; afterwards the electrode B1 was set to 0 volts and the bias voltage applied to the electrode A1

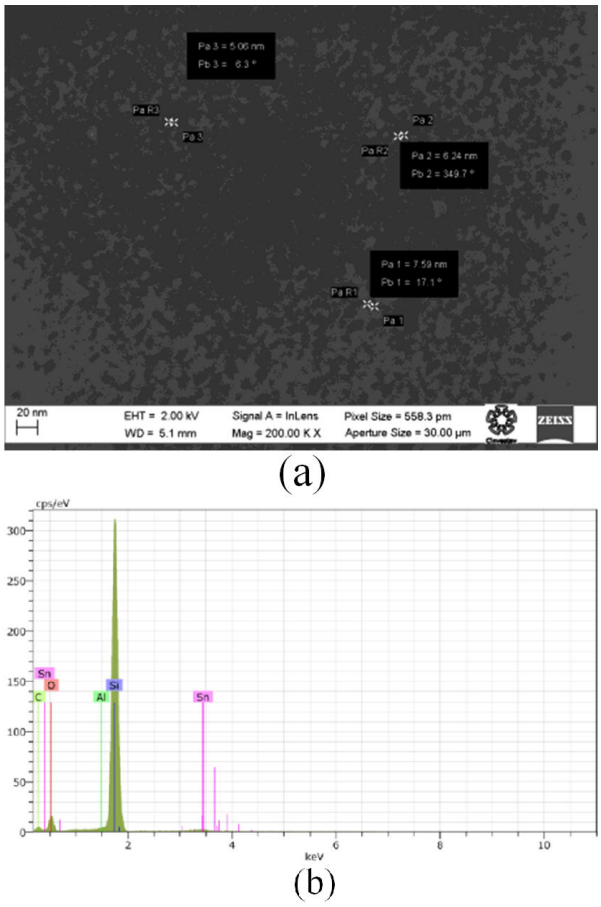

FIGURE 3. (a) SEM microphotograph on the Point 2 with a 200.00 X magnification to illustrate the surface topography of the PS film arranged with a distribution of porous and remaining silicon zones, the dark regions were identified as porous with diameters ranging from 5 to 7.59 nm. (b) Typical EDS analysis for the PS regions showing that the films are mainly formed by silicon.

A1 was swept from 0 volts up to a positive voltage, V^+ volts. The second mode was applied after 10 seconds considering that during this period the traps retain its charge state; subsequently the bias voltage applied to the electrode A1 was swept from V^+ toward 0 volts.

3. Results and Discussion

The surface of the resulting PS films produced by electrochemical etching has mirror-like appearance to the naked eye. Figures 2 and 3 show two scanning electron microscopy (SEM) microphotographs of the typical PS surface samples. Figure 2a) shows a microphotograph with 198X magnification at the border of the Au electrode, the Point 4 is over the Au contact and the Points 1-3 are located on the PS surface. Figure 2 b) is a microphotograph with 50.00 X magnification of the Point 2 showing no apparent features on the PS surface. The Fig. 3 a) is microphotograph with 200.00 X magnification at the point 2; with this amplification the porous features of the PS film are clearly visible showing large porous of

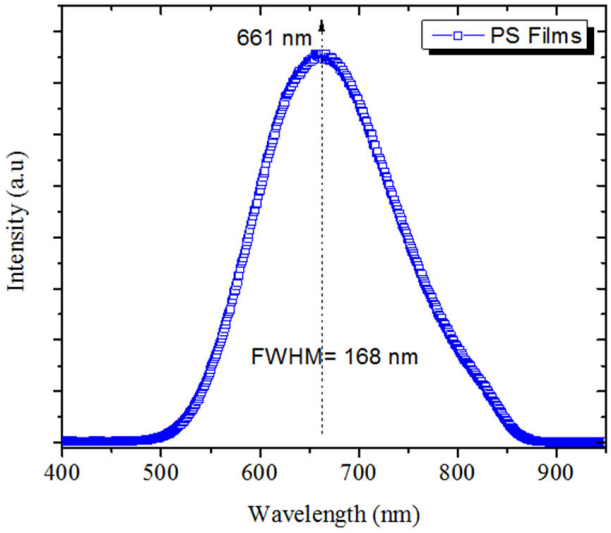

FIGURE 4. PL spectrum obtained from the PS films at room temperature.

diameters 5 to 7.59 nm accompanied by a distribution of voids with less diameter conforming with the remaining crystalline silicon regions the well- known nano-crystalline silicon structure. Figure 3 b) includes a typical EDS analysis of the PS regions showing that the films are mainly formed by silicon with oxygen content under 5 % atomic.

Figure 4 shows the PL spectrum produced by the PS films; the luminescence excited by a UV lamp is of dark-red color with its maximum located at the wavelength of 661 nm with a full width at half maximum (FWHM) of 168 nm, the PL spectra is similar to the ones reported elsewhere [12]. The intense and stable PL response has been well justified by quantum confinement effects produced by the nanocrystallites constituting the PS films [13]. According to diverse PL studies the PS films is comprised by a network of silicon nano- crystallites with sizes spreading from 1.5 to 4 nm [14,15]. The SEM analysis done in the samples used in this study show easily observable porous silicon with diameters below 7.9 nm uniformly distributed over the PS surface, in line with the diameters estimated from PL measurements.

The electrical characterization of the PS films was done using the electrodes depicted in Fig. 1 selecting distinct pairs of motifs. With the I-V measurements taken between pairs of electrodes, A1 and B1 for example and the geometrical dimensions of the PS films a resistivity of 4.48×10^9 Ω-cm was calculated in accordance with the reported data in the literature [16]. The linear representation of the current-voltage (I-V) characteristic depicted in Fig. 5 shows similar appearance to the ones described in the reference [17]. In our case the observed asymmetry is justified in first instance by the high resistivity of the PS films bounded by the pair of Au/PS electrodes. It must be pointed out that the typical separation distance between the nanocrystallites in the PS films is of few nanometers according to the reported results in the literature [18] and our previously described SEM analysis; the

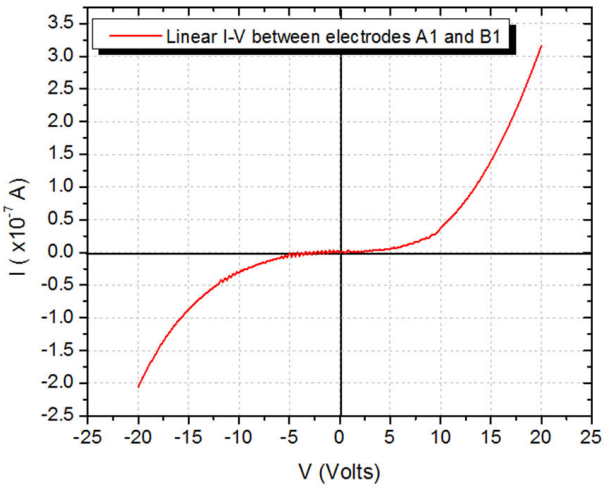

FIGURE 5. Linear representation of the current-voltage (I-V) characteristics measured between electrodes A1 and B1 in the Au/PS/Au structure.

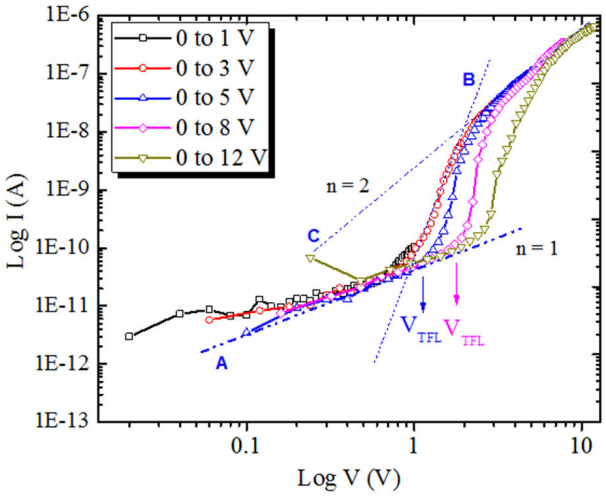

FIGURE 6. Forward bias $\log I - \log V$ plot characteristics for the first mode measurement measured in Au/PS/Au structures beginning with the empty traps condition at $V = 0$.

the EDS analysis also demonstrates that the nano-crystalline silicon skeleton is covered by a thin SiO_x film. Therefore the possible current transport mechanisms in the PS films must necessarily include mechanisms such as hopping, as well as the carrier activation from localized defect states and the Poole-Frenkel effect driven by intense local electric fields at the distinct sites within the PS film [8].

The I-V characteristics in the $\log I - \log V$ plot produced by applying the first and second measurement modes applied to the planar structures are represented in Fig. 6 and 7, respectively. The groups of curves included were obtained by applying bias voltages with the ranges marked in the corresponding insets.

Over the set of I-V curves shown in Fig. 6 a triangular area limited by lines A, B and C is drawn; each line fits well over a wide range on the experimental curves. The line A with the lower slope matches with the Ohmic behavior ($I \sim V$); as is usual this mechanism prevails at lower electric

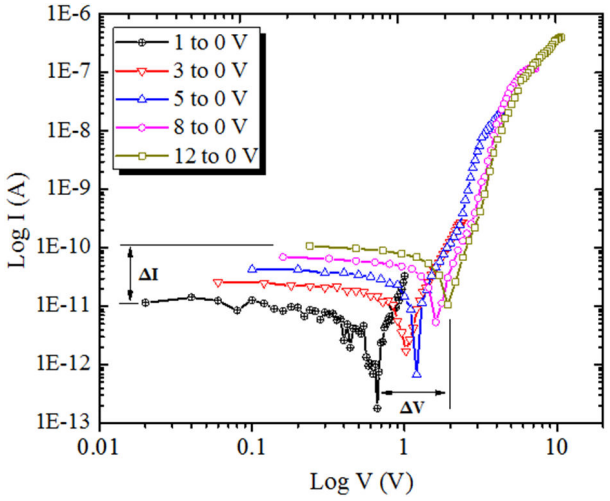

FIGURE 7. Forward bias $\log I - \log V$ plot characteristics for the second mode measurement measured in the Au/PS/Au structure beginning with the full traps charge condition.

fields. Then, as the applied bias range was increased, the current rises at a high rate; for the ranges of bias voltage used a set of curves with the common slope B were produced, but each curve shifts to the right as the fixed voltage bias maxima V^+ was increased. The voltage where the Ohmic behavior ends and the rate of change in the current abruptly increase, for example with the slope B, corresponds to the trap-filled limit voltage (V_{TFL}) usually identified in wide band gap insulating materials.

The measured I-V curves resulted stable and reproducible; therefore, in our samples when the bias voltage maximum was extended, the V_{TFL} shifts steadily toward higher values. Later on as the field was further increased the rate of change in the current decreases following the line with slope C; the line to fulfill the triangular area is produced by extending the trace according to the function $I \sim V^2$ toward lower voltages. The mechanism described by the line C at higher fields corresponds to the space charge limited current (SCLC) regime [19]. Therefore, the superposed triangular-like shape drawn over the measured $I - V$ characteristics demonstrates that the carrier transport in the PS films is controlled by the trapping kinetics of the thermally generated carriers in the PS and the SCLC regime due to ionized traps. These mechanisms are ordinarily seen in diverse highly defective large band-gap materials [20].

The functions representing the boundary lines limiting the triangular shaped area depicted on Fig. 6 can be properly described as follows. The current density produced at low electric fields varies according to Eq. 1 [19,20]:

$$J = qp_0\mu_p\frac{V}{d} \tag{1}$$

where p_0 is the concentration of the thermally generated holes, μ_p their mobility at low electric fields, V the applied voltage between the electrodes separated by the distance d,

and q the electronic charge. p_0 and μ_p are the electrical parameters of the PS films at low electric fields; in carrier injection conditions the hole concentration p and μ_p changes accordingly.

After the Ohmic region, the presence of trap energy levels modifies the rate of change of the current, in our case according to the slope B as is seen in Fig. 6. The bias voltage where the line with slope A traverses the line with slope B defines the trap-filled limit voltage (V_{TFL}); for single level traps their concentration N_t is related to V_{TFL} by the Eq. 2 [21,22]:

$$V_{\text{TFL}} - \frac{qN_t d^2}{\varepsilon_s} \tag{2}$$

where ε_s is the material dielectric constant and d the separation distance between the electrodes. As was pointed before a clear shift in the V_{TFL} toward higher voltages is produced as the voltage bias maxima V^+ was extended suggesting an increase on N_t; however, as the trap concentration must be constant, the observed shift on V_{TFL} can be explained by the microscopic nature of the PS films and the traps properties either in the bulk or the surface. It can be suggested that the V_{TFL} shift is produced by to the existence of multiple level energy traps activated by the biasing mode conditions. Reports describing analogous shifting on V_{TFL} on diverse materials have been justified by material phase transitions, or structural modifications produced by thermal annealing processes, for example in SiO_2 layers doped with Er [23]. At the authors knowledge this is the first work reporting the identification of V_{TFL} in PS films, the V_{TFL} shifting can be explained by the delay of the charge emission or the charge detrapping, producing the apparent increase in the trap density (N_t), suggesting the occupation kinetics of the excited energy levels.

The influence of excited energy levels can be justified by changes in the trap potential energy configuration produced by carrier trapping during the bias sweeping stage. This effect is linked to charge loading processes observable by time periods elapsing from some seconds to minutes, or several hours according to the material and traps properties.

Finally, the line with slope C corresponds to the current variation as the square of the applied bias voltage described by the Eq. 3.

$$J = \frac{9}{8}\varepsilon_s \mu_p \frac{N_v}{N_t(s)} \exp\left(\frac{-E_t}{kT}\right)\frac{V^2}{d^3} \tag{3}$$

where N_v is the effective density of energy states in the valence band, $N_t(s)$ is the density of single level traps with energy E_t. This behavior is characteristic of the carrier transport where the carrier dispersion is mainly produced by ionized traps [24,25]. It must be pointed out that at high bias all the I-V curves returns to equal values described by Eq. 3.

Furthermore, in presence of distributions of diverse energy levels Eq. 4 is used to consider the occupation factor θ of the dominant traps, the Eq. 4 is regularly used [24].

$$\theta = \frac{N_v}{N_t(s)} \exp\left(\frac{-E_t}{kT}\right) \tag{4}$$

Because the occupation kinetics is electric field dependent, the $\log I - \log V$ plots must vary according to the properties of the PS traps. As the electrical current behavior is also affected by the nature of the surfaces or by possible adsorbed environmental gaseous species, the experimental $I - V$ characteristics could acquire diverse appearance according to the material history and by changes on film properties as the permittivity, carrier mobility and phase stability.

By replacing the Eq. (4) into the Eq. (3) the current flow at higher fields can be expressed according to Eq. 5.

$$J = \frac{9}{8}\varepsilon_s \mu_p \theta \frac{V^2}{d^2} \tag{5}$$

Equations 1 to 5 have been used to explain the behavior of a variety of nanometric structures; for those cases the influence of the electrodes location acquire relevance because the distance d is considerably reduced in comparison with this work. As is described in Ref. 26, a number of cases correspond to single energy level traps having exponential energy levels distributions function according to the Eq. 6.

$$N_t(q) = \frac{p_0}{T_c} \exp\left(\frac{-E_t}{kT_C}\right) \tag{6}$$

where p_0 is the hole concentration, T_c the characteristic temperature and k the Boltzmann's constant. Using this model M. A. Rafiq *et al.* [27] found a $T_c \sim 1670$ K for nanocrystalline silicon film structures through the analysis of the $I-V$ characteristics in the high electric field regime, where the SCLC mechanism clearly predominates. The traps distributions should also modify the $I-V$ characteristics appearance; for a Gaussian trap distribution the described triangular-like shape clearly modifies [28]. In complex materials like the composites, were changes in the effective length between the test electrodes are usually produced, is necessary to consider variations in geometry and the structures configuration, therefore distinct authors have proposed modifications to the pre-

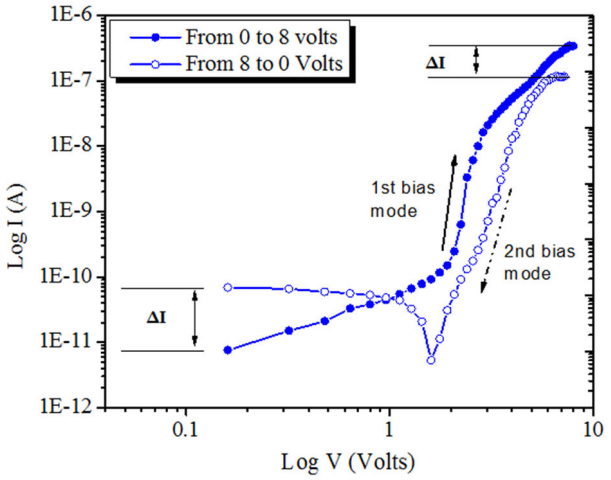

FIGURE 8. Forward bias $I - V$ curves for both initial charge trap conditions to illustrate the general electrical behavior of the Au/PS/Au structures.

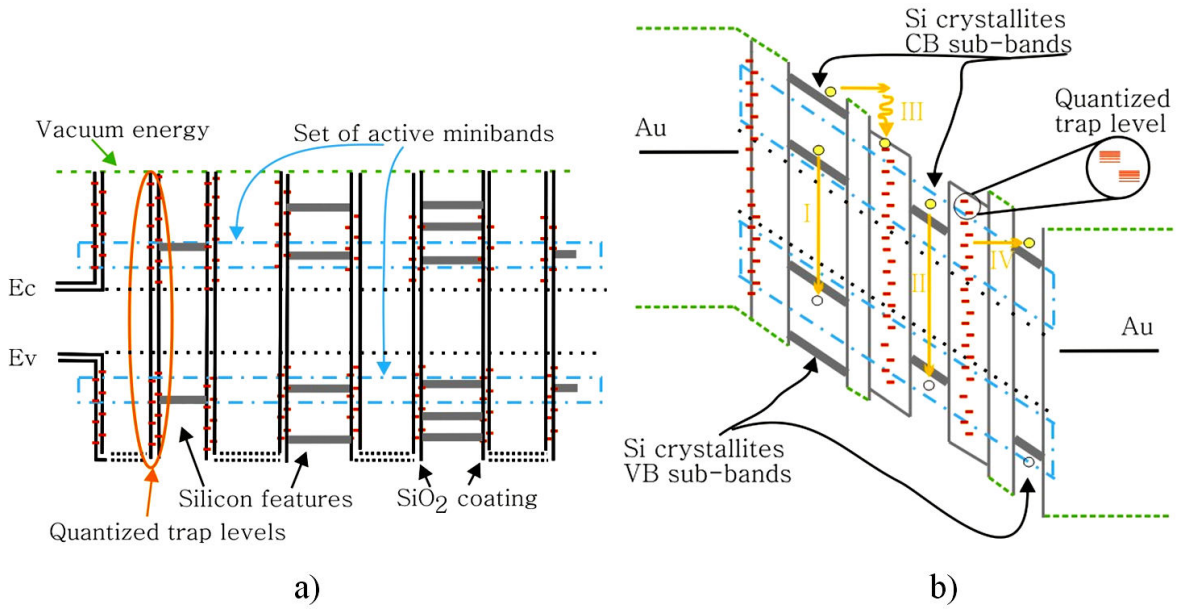

FIGURE 9. (color on line) Band diagram sketch of both PS films in thermal equilibrium (a) and the Au/PS/Au structure under applied bias (b). In the Fig. 6b, different recombination process are depicted [I).- Radiative recombination and II).- Nonradiative recombination (Auger, Trap/SRH)] and the transport mechanism produced under an applied bias [III).- Carrier capture and IV).- Tunneling].

vious to the previous model. The characteristic $I-V$ behavior at higher fields where the SCLC mechanism dominates has the general form given by Eq. 7 [26]:

$$q\mu N_v \left(\frac{\varepsilon_s}{p_0 T_C}\right) \frac{V^{l+1}}{d_{eff}^{2l+1}} \tag{7}$$

where the exponent is $n = l+1$ and usually $(l+1) > 2$. The meaning of the parameter l is T_c/T, where T is the absolute temperature, T_c the trapping characteristic temperature [29] and d_{eff} is an effective length between electrodes.

Finally, the $\log I - \log V$ characteristics produced with the second measurement mode is shown in the Fig. 7. Two noticeable behaviors are revealed; a clear inversion in the rate of change of the electrical current at positive bias voltages and the clamping of the current in a positive value driven by the maxima bias voltage chosen in the sweeping process.

The inversion in the rate of change of the current flow while the bias voltage was swept to cero volts can be explained by the de-trapping process; the condition where the current minima is produced is within a voltage range ΔV. The observed minima in the current at bias voltages around 1 volt suggest that the dominant traps levels are located around the half of the effective PS electrical bandgap. The negative slope produced by the detrapping process produces a negative resistance effect that can be interpreted as a virtual current source. The intensity of the current source correlates to the maximum bias voltage used in the second mode sweeping. As can be observed in Fig. 7 the maximum current produced is $\Delta I \sim 1 \times 10^{-11}$ A.

To summarize the discussed behavior the pair of $I-V$ curves produced with both measurement modes using the voltage ranges from 0 to 8 volts and from 8 to 0 volts were included in the Fig. 8. It is convenient to point out that the trap centers in the PS are diverse and distributed either into the PS surfaces or at the Au/SiO_x/PS interfaces.

The previous described results behavior was observed on several series of our characterized planar Au/PS/Au structures with PS films produced with described procedure. To the best of our knowledge this is the first complete report describing the controllable phenomena with PS films.

On the basis of the described results, the Fig. 9 shows a possible energy band diagram of the studied structure in thermal equilibrium (a) and under applied bias (b) where the distinct recombination paths into the PS are depicted. In the Fig. 9a, the different energy levels related to the nature of the PS film are included to describe the observed behavior on the $I-V$ characteristics. The vacuum energy level, the discrete energy levels provoked by the existent non-stoichiometric SiO_x and the build-up sub-band generated by the quantization produced by the silicon nanocrystallites in the PS films, represented by the blue rectangles, are depicted. The conduction and valence bands are represented as the continuous line. However, the effective bandgap of the PS films should be represented according to the sub- band generated by the size effects of the silicon nanocrystals. In the scheme of Fig. 9 the discrete energy levels within the non-stoichiometry silicon oxide are also represented because these centers are responsible of the slow emission kinetics. In bias voltage conditions, the situation represented in the Fig. 9b is produced, where some changes on the trapping-detrapping paths are considered.

4. Conclusions

Au/PS/Au structures build with PS layers of 60 nm in thickness and resistivity of 4.48×10^9 Ω-cm. The PS films are considered as a network-like-silicon-nanocrystallites covered by a non-stoichiometry silicon oxide film. It was found that the carrier transport is controlled by the SCLC mechanism combined with the charge trapping-detrapping kinetics in the different defect centers of the PS films. The behavior of the $I-V$ curves change according to the initial charge state condition, the magnitude and rate of change of the applied bias voltage. An equivalent V_{TFL} was identified for the PS films that shift within the voltage range of 1 to 3 volts; the shifting effect on the V_{TFL} demonstrates the existence of multiple energy level traps in the PS films. Particular behavior was found in the region of low bias voltage by the trapping-detrapping charge effects with the participation of deep level centers of density Nt, produced by the initial charge trap state conditions used in this work. The detrapping charge kinetics was interpreted as a buildup of a virtual current source in the range of $\Delta I \sim 1 \times 10^{-11}$ Amp driven by the bias voltage used. An energy band diagram is proposed to represent the trapping-detrapping of the PS films according to the initial charge state conditions.

Acknowledgments

We want to acknowledge M. Sc. Miguel Galván Arellano for the valuable technical support. The authors acknowledge the Ph.D. Jorge Roque De La Puente for SEM imaging and EDS support at Cinvestav (LANE).

1. G. K. Celler and S. Cristoloveanu, *J. Appl. Phys.* **93** (2003) 4955.
2. L. Zhu, J. Zhou, Z. Guo, and Z. Sun, *J. Materionmics* **1** (2015) 285.
3. K. Ueno and N. Koshida, *Appl. Phys. Lett.* **74** (1999) 93.
4. G. Korotcenkov, *Porous silicon: From formation to applications*. CRC Press, Boca Raton, USA (2016).
5. V. Pacebutas, K. Grigoras and A. Krotkus, *Physica Scripta* **T69** (1997) 255.
6. M. J. Sailor, *Porous silicon in practice, preparation characterization and applications*. (WILEY-VCH Verlag Gmbh & Co. kGaA, 2011).
7. K. Grigoras, J. Keskinen, L. Grönberg, J. Ahopelto and M. Prunnila, *ECS Trans.* **75** (2016) 97.
8. J. Das, S. Pradhan and S. M. Hossain, *J. Nanomater. Mol. Nanotechnol.* **2** (2016) 5.
9. H. Hagino, S.Tanaka, N.Tanimura, K. Miyazaki, *Int. J. Thermophys.* **36** (2015) 2548.
10. R. Schwarz, F. Wang, M. Ben-Chorin, S. Grebner, A. Nikolov and F. Koch, *Thin Solid Films* **255** (1995) 23.
11. M. A. Vásquez-A, G. Romero-Paredes, J.A. Andraca-Adame and R. Peña-Sierra, *Rev. Mex. Fís.* **62** (2016) 5.
12. E. Díaz-Torres, G. Romero-Paredes, R. Peña-Sierra, A. Ávila-García, *Materials Science in Semiconductor Processing* **40** (2015) 533.
13. M. A. Vásquez-A, G. García Salgado, G. Romero-Paredes and R. Peña-Sierra, *Rev. Mex. Fís.* **53** (2007) 431.
14. M. V. Wolkin, J. Jorne, P.M. Fauchet, G. Allan, and C. Delerue. *Phys. Rev. Lett.* **82** (1999)197.
15. V Lehmann, B Jobst, T Muschik, A Kux and V Petrova-Koch, *Jpn. J. Appl. Phys.* **32** (1993) 2092.
16. S. Ménard, A. Févre, J. Billoué and G. Gautier, *J. Appl. Phys.* **118** (2015) 105703.
17. G. Micard, K. Peter, D.Chrastina, G.Isella, *Proc. 22nd EU PVSEC* (Milan 2007) 2169.
18. O. Bisi, Stefano Ossicini, L. Pavesi, *Surface Science Reports* **38** (2000) 1.
19. F.-C. Chiu, *Advances in Materials Science and Engineering* **2014** (2014) Article ID 578168.
20. P. Mark and W. Helfrich., *J. Appl. Phys.* **33** (1962) 205.
21. D. B. Dimitrov, *Physical Review B* **51** (1995) 1566.
22. M. A. Lampert, *Physical Review* **103** (1956) 1648.
23. O. Jambois *et al*., *J. Phys. D: Appl. Phys.* **45** (2012) 045103.
24. T. Matsumoto, H. Mimura, N. Koshida, and Y. Masumoto, *J. Appl. Phys.* **84** (1998) 6157.
25. M. L. Ciurea *et al*., *Appl. Phys. Lett.* **76** (2000) 3067.
26. M. A. Lampert and P. Mark, *Current Injection in Solids* (Academic Press, Inc., New York, NY, 1970).
27. M. A. Rafiq *et al*., *Appl. Phys. Lett.* **87** (2005) 182101.
28. H. T. Nicolai, M. M. Mandoi and P. W. M. Blom, *Physical Review B* **83** (2011) 195204.
29. A. Jain *et al*., *J. Appl. Phys.* **102** (2007) 094505.